

Gas Adsorption and Dynamics in Pillared Graphene Frameworks

Andrea Pedrielli^{a,b}, Simone Taioli^{b,c,*}, Giovanni Garberoglio^{b,**}, Nicola Maria Pugno^{a,d,e}

^aLaboratory of Bio-Inspired and Graphene Nanomechanics, Department of Civil, Environmental and Mechanical Engineering, University of Trento, Via Mesiano 77, 38123 Trento, Italy

^bEuropean Centre for Theoretical Studies in Nuclear Physics and Related Areas (ECT*-FBK) and Trento Institute for Fundamental Physics and Applications (TIFPA-INFN), 38123 Trento, Italy

^cFaculty of Mathematics and Physics, Charles University, 180 00 Prague 8, Czech Republic

^dSchool of Engineering and Materials Science, Queen Mary University of London, Mile End Road, London E1 4NS, United Kingdom

^eKet Lab, Edoardo Amaldi Foundation, Italian Space Agency, Via del Politecnico snc, 00133 Rome, Italy

Abstract

Pillared Graphene Frameworks are a novel class of microporous materials made by graphene sheets separated by organic spacers. One of their main features is that the pillar type and density can be chosen to tune the material properties. In this work, we present a computer simulation study of adsorption and dynamics of H₂, CH₄, CO₂, N₂ and O₂ and binary mixtures thereof, in Pillared Graphene Frameworks with nitrogen-containing organic spacers. In general, we find that pillar density plays the most important role in determining gas adsorption. In the low-pressure regime ($\lesssim 10$ bar) the amount of gas adsorbed is an increasing function of pillar density. At higher pressures the opposite trend is observed. Diffusion coefficients were computed for representative structures taking into account the framework flexibility that is essential in assessing the dynamical properties of the adsorbed gases. Good performance for the gas separation in CH₄/H₂, CO₂/H₂ and CO₂/N₂ mixtures was found with values comparable to those of metal-organic frameworks and zeolites.

Keywords: Nanomaterials, Molecular Dynamics, Gas adsorption, Porosity

1. Introduction

In order to exploit graphene for gas adsorption and mechanical applications, many different kinds of 3D carbon-based structures were proposed in the past years, such as carbon nanotube networks (Ding et al., 2007), carbon nanoscrolls (Mpourmpakis et al., 2007; Coluci et al., 2007) and graphene foams (Alonso, 2012; Pedrielli et al., 2017). At the same time, a growing interest was shown to materials in which graphene is enhanced by chemical functionalization or the addition of external components such as organic molecules (Tang et al., 2013). In this last category, Pillared Graphene Frameworks (PGF) are a novel class of materials, composed by stacked graphene layers separated by organic moieties.

Analogously to Pillared Graphene-Oxide Frameworks (PGOF) (Srinivas et al., 2011; Kumar et al., 2014), the properties of PGFs can be varied by changing the kind and the density of organic spacers hence obtaining a fine tuning of gas absorption and gas separation performances. Similarly to other materials for gas adsorption such as Metal Organic Frameworks (MOFs), (Duren et al., 2004; Babarao et al., 2007; Duren et al., 2009; Colon and Snurr,

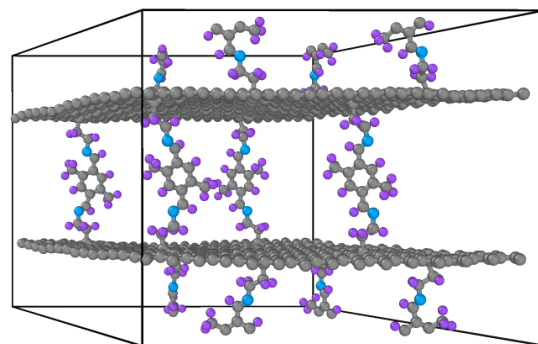


Figure 1: View of a Pillared Graphene Framework. The pillars are constituted by organic molecules covalently bonded to graphene layers. Carbon atoms are rendered in grey, hydrogen in violet and nitrogen in blue.

2014) Zeolitic Imidazolate Frameworks (ZIFs), (Battisti et al., 2011; Zhang et al., 2013) and PGOFs (Burruss et al., 2010; Garberoglio et al., 2015), the gas adsorption and separation performances of PGFs can be fruitfully studied by means of computer simulations (Wang et al., 2014).

However, gas adsorption and separation in PGFs are still largely unexplored despite their ease of fabrication with respect to other metallic frameworks. In this work, we investigate these properties for a class of structures in which the spacers are nitrogen-containing organic molecules using Grand Canonical Monte Carlo (GCMC)

*Second corresponding author

**First corresponding author

Email addresses: taioli@ectstar.eu (Simone Taioli), garberoglio@ectstar.eu (Giovanni Garberoglio)

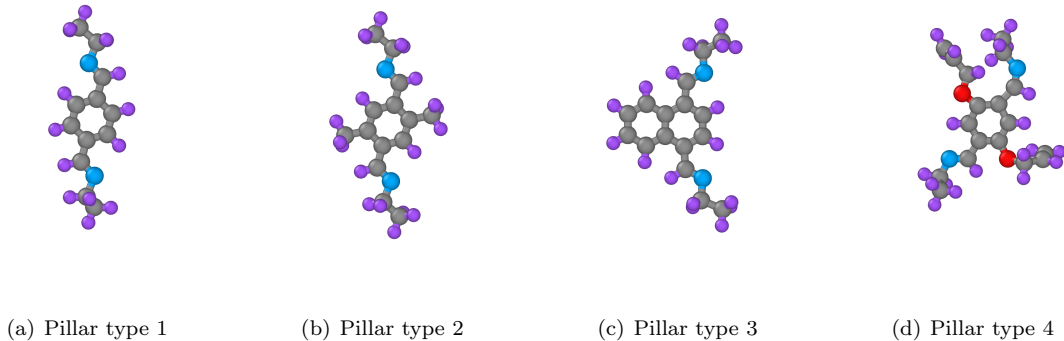


Figure 2: The four nitrogen-containing organic pillars considered in this work. Carbon atoms are rendered in grey, hydrogen in violet, nitrogen in blue and oxygen in red.

and Molecular Dynamics (MD) simulations. The principal goal of this work is to investigate the role of pillar type and pillar density in determining the performance of PGFs for gas adsorption and gas separation. In particular, we will investigate whether the quantity of gas adsorbed can be optimized by varying the density of pillars. In fact, one could expect adsorption increase with the number of pillars at small pillar density (providing more adsorption sites), whereas adsorption high pillar density could be prevented by progressive lack of available volume. Consequently, there might be a specific pillar density optimizing gas uptake.

Furthermore, the influence of pillar density and type on gas separation performances will be assessed. The gas separation performance for a gas mixture depends in general from two main factors: first the gas adsorption of a gas with respect to the other, namely the gas selectivity, second the difference in the diffusion coefficient of the two species. To estimate the gas separation performances of PGFs we will compute the gas selectivity for different mixtures as well as the diffusion coefficients for single component gases.

In computing the diffusion coefficients and assessing the dynamical properties of the adsorbed gases the flexibility of the adsorbent can strongly influence the simulation results, as shown for other materials (Battisti et al., 2011; Zhang et al., 2014). Due to the high mobility of the structure considered in this work, we took into account structural flexibility in all dynamical simulations.

2. Computer model

Pillared Graphene Frameworks are composed by stacked graphene layers separated by organic spacers. Here we investigate a narrow class of these structures with four types of nitrogen-containing organic spacers. For each type of organic spacer we generated several computational samples with various pillar density, between 0.09 and 1.71 pillars nm^{-2} . We report in Fig. 1 a sketch of an entire sam-

ple. In Fig. 2, the four types of organic pillars considered in this work are shown.

Pillar Type	Pillar Density (nm^{-2})	Free Volume (%)	Mass Density (g cm^{-3})
1	0.09	77.1	0.443
	0.68	67.9	0.555
	1.37	57.1	0.687
2	0.09	76.5	0.450
	0.68	65.8	0.569
	1.37	52.7	0.721
3	0.09	74.5	0.490
	0.68	65.5	0.585
	1.37	51.0	0.755
4	0.09	71.0	0.560
	0.68	55.5	0.731
	1.37	38.9	0.942

Table 1: Free volume and mass density for the samples with pillar type 1 to 4 and with representative pillar density. The free volume is defined in Eq. (1).

In generating computational supercells, we prepared a hexagonal unit cell with periodic boundary conditions containing two graphene layers with base vectors $a = b = 3.684 \text{ nm}$ intercalated by the organic molecules, in such a way that the pillars were alternated in their anchorage to successive graphene planes (see Fig. 1). The length of the third base vector c , perpendicular to the graphene planes, was set to accommodate the pillars, approximately 3 nm for all the pillar types. Free volume and mass density for the samples with pillar type 1 to 4 and with representative pillar density are reported in Tab. 1.

To conclude the preparation of the samples, we equilibrated them using the LAMMPS program (Plimpton, 1995) by means of 50 ps isothermal-isobaric Molecular Dynamics simulations at room conditions, using the ReaxFF potential (van Duin et al., 2001; Chenoweth et al., 2008)

with parameters suitable for organic molecules and carbon-based materials (Mattsson et al., 2010). For each sample, we saved one equilibrated configuration of atomic coordinates to be used in the subsequent studies. Furthermore, we saved the point charges that were self-consistently calculated during the ReaxFF simulation (QEq method (Nakano, 1997; Rappé and Goddard, 1991)), and we used these point charges in all the simulations in which Coulomb interaction had to be taken into account.

To investigate gas adsorption and separation in these materials we used the Grand Canonical Monte Carlo Method. For a detailed description of the method we refer the reader to a previous paper (Battisti et al., 2011). In GCMC, as well as in Molecular Dynamics simulations, it is necessary to choose a model for both the gas-gas and the gas-adsorbent interaction. Here we described the molecules as rigid rotors interacting via Lennard-Jones sites and point charges. In particular we used the EPM2 potential for CO₂ (Harris and Yung, 1995), and the parameter validated by Murthy for N₂ (Murthy et al., 1980) and by Zhang (Zhang and Siepmann, 2006) for O₂. With regard to CH₄ and H₂ we used a single-site Lennard-Jones potential, with the parameters validated by Buch (Buch, 1994) and Goodbody (Goodbody et al., 1991), respectively. The pure-fluid phase diagram is well described by these models.

The commonly used DREIDING (Mayo et al., 1990) force field, augmented with the ReaxFF framework charges, was used to describe the gas-adsorbent interaction. Another popular choice is the UFF force field (Rappé et al., 1992), which we considered for some cases. Analogously to other studies appeared in the literature, we also found that UFF generally results in higher adsorption quantities than DREIDING (Garberoglio et al., 2005; Sumida et al., 2012; Getman et al., 2012). The cutoff of the long range van der Waals and Coulomb gas-adsorbent interactions was set to 1.6 nm.

Framework flexibility could have strong effects on molecular transport in materials with small window sizes or soft components whereas in rigid structures with large pores has minor effects (Amirjalayer et al., 2007; Haldoupis et al., 2010; Hertag et al., 2011; Pantatosaki et al., 2012).

For the materials considered in this work the pore size as well as the structural rigidity is dependent on the pillar density so that the mobility of the adsorbent during the gas diffusion simulations has to be taken into account. Hence, we used the bonded part of the UFF force field to describe framework flexibility, keeping the DREIDING parameters to describe long-range dispersive interactions. Recent calculations have shown that UFF is very efficient yet capable to describe a broad range of microporous materials with reasonable accuracy (Garberoglio and Taioli, 2012). Indeed, in some preliminary tests, we found that if the framework is kept rigid the underestimation of the diffusion coefficient can be up to 40 % lower, when high pillar density structures are considered. In both GCMC and MD simulations the Lorentz–Berthelot mixing rules were

used to calculate the long range van der Waals interaction between unlike atoms.

3. Results and Discussion

3.1. Pure-fluid isotherms

Pure fluid isotherms were computed for H₂, CH₄, CO₂, N₂ and O₂ gases. The van der Waals equation of state was used to relate the chemical potential to the pressure of the reservoir gas using parameters set to reproduce the position of the adsorbate critical point (Hirschfelder and Curtiss, 1954). For each external pressure we performed 5×10^5 equilibration steps (one step being an insertion, a deletion, or a translation/rotation of an already adsorbed molecule, all performed with equal probabilities), followed by 1 million production steps.

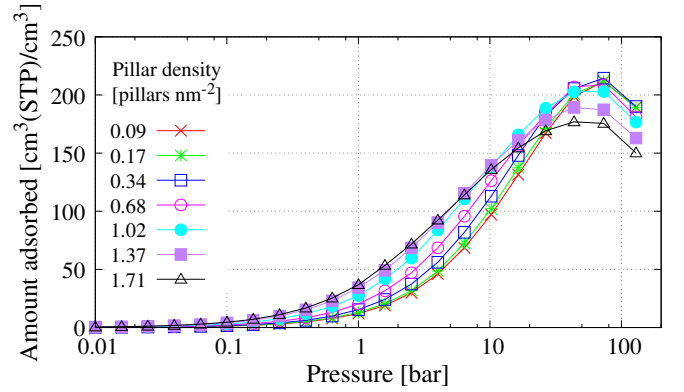


Figure 3: Volumetric adsorption isotherms of CH₄ at T= 298 K for pillar type 1.

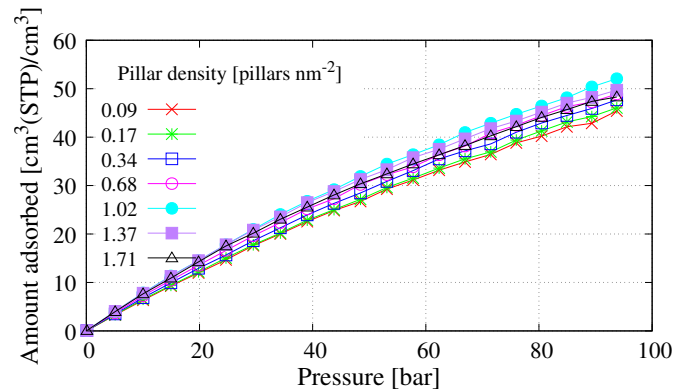


Figure 4: Volumetric adsorption isotherms of H₂ at T= 298 K for pillar type 1. The best uptake is obtained for an intermediate pillar density of 1.02 pillars nm⁻².

In particular, we computed the excess amount, N_{ex} , that can be obtained by estimating the number density $\rho(T, P)$ of the adsorbate at the given thermodynamic condition (calculated using the van der Waals equation of state) and the available free volume for the adsorption V_{free}

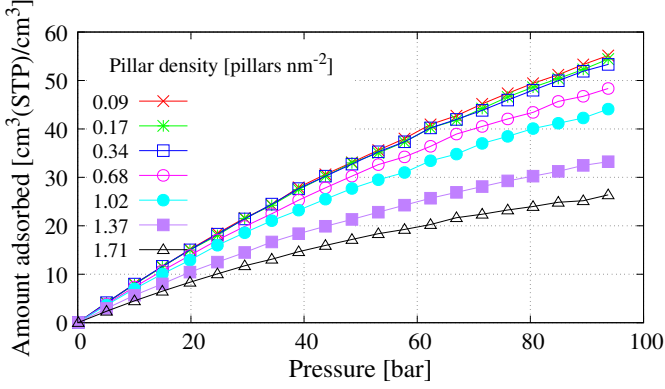


Figure 5: Volumetric adsorption isotherms of H_2 at $T= 298$ K for pillar type 4. As the pillar density decreases the adsorption uptake increases.

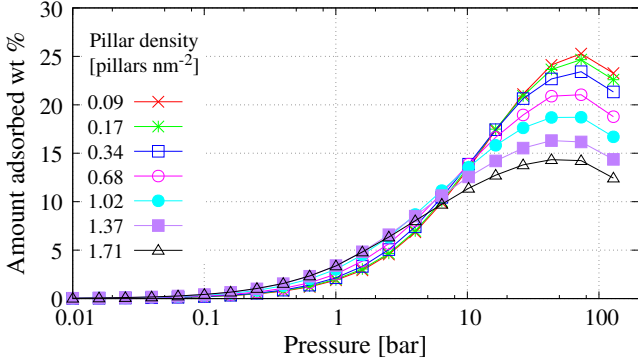


Figure 6: Gravimetric adsorption isotherms of CH_4 at $T= 298$ K for pillar type 1. At high pressure, near the saturation limit, we found a clear performance decrease as pillar density increases, the contrary happens at low pressure.

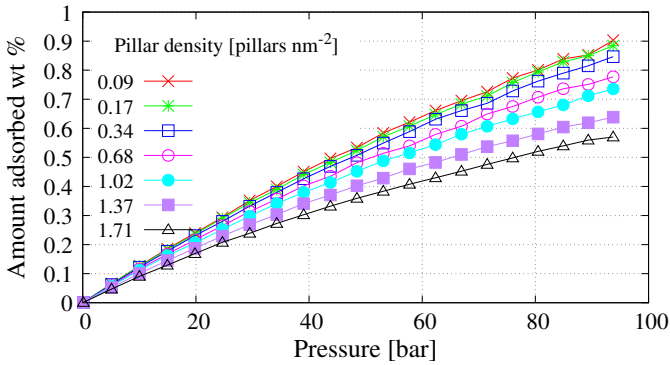


Figure 7: Gravimetric adsorption isotherms of H_2 at $T= 298$ K for pillar type 1. As the pillar density decreases the adsorption uptake increases. The saturation is not reached within 100 bar.

(Hirschfelder and Curtiss, 1954). The free volume is conventionally defined as the volume of the region where the solid-gas interaction between the framework and a helium atom divided by the Boltzmann constant k_B is less than 10^4 K. The excess number of adsorbed molecules is then defined as

$$N_{\text{ex}} = N - \rho(T, P) V_{\text{free}}, \quad (1)$$

where N is the total number of gas molecules.

It is in general useful to define two kinds of isotherm curves. The first one is the volumetric isotherm which is given by the ratio between the volume occupied by the adsorbed gas at standard pressure and temperature, and the geometric cell volume. This measure of adsorption indicates how much the presence of the adsorbent can concentrate within the adsorbate with respect to room conditions. The second kind is the gravimetric isotherm and is given by the percent ratio between the weight of the adsorbed gas and the sum of the weights of the framework and the adsorbed gas. This quantity is of practical interest for fuel storage, especially for automotive applications where the weight of the system is of particular concern.

For all the gases (H_2 , CH_4 , CO_2 , N_2 , and O_2), adsorption isotherms were computed at 298 K. In the case of H_2 we also considered $T = 77$ K. In what follows, we will focus mainly on isotherms for the pillar type 1 reporting in the Supplementary Information the results for the other pillar types, because we generally found minor differences as a function of the pillar type.

Some features of these isotherms are common to almost all the cases investigated in this paper. Referring to the volumetric adsorption isotherm of CH_4 at 298 K reported in Fig. 3, one notices that at low pressures (roughly below 10 bar) the quantity of gas adsorbed increases up to two times with increasing pillar density. Indeed, visual inspection of the GCMC configurations shows that in this regime gas is mostly adsorbed close to the framework atoms and a larger number of pillars provides more adsorption sites. This trend was found for all gases except H_2 at 298 K, independently of the pillar type.

Conversely, for larger pressures, the amount of gas adsorbed is a decreasing function of the density of pillars. In this regime, the gas is also adsorbed in the volume between the pillars, but the volume available for adsorption decreases with increasing pillar density due to steric hindrance. Because the maximum volumetric uptake was found for the samples with lower pillar density, the maximum uptake is in general independent of pillar type. In fact, for high pressure, the maximum uptake is essentially limited by the total free volume, that decreases as the pillar density increases.

The volumetric adsorption isotherms of H_2 , reported in Fig. 4, do not follow this general picture. First of all, even at the highest pressure investigated here (100 bar) there is no sign of reaching saturation.

However, despite being in the “low-pressure regime”, the dependence of the amount adsorbed with respect to the

pillar density does not follow the trend observed in the case of the other gases, for one sees that there is an optimal pillar density (around 1 nm^{-2}) that optimizes adsorption, although volumetric uptake is similar (within 20%) for all the considered pillar density. The same optimal pillar density was found for PGFs with pillar type 2 and 3. In the case of samples with pillar type 4, reported in Fig. 5, this optimal pillar density is not present and we found the uptake being a decreasing function of pillar density. This kind of behavior is related to the high pillar volume of the pillar of type 4, resulting in the lack of free volume also for low pillar density samples.

Gravimetric gas adsorption isotherms at $T = 298 \text{ K}$ for the various structures containing pillars of type 1 and different pillar density are shown in Fig. 6 and 7 in the case of CH_4 and H_2 , respectively. In the case of CH_4 the isotherms display the same qualitative behavior observed in the volumetric case: adsorption increases with pillar density for low pressures, and decreases at higher ones. However, in this case the normalization with the total mass of the system enhances the difference in adsorption at high pressures, while diminishing it in the low-pressure regime.

For H_2 gravimetric isotherms, reported in Fig. 7 at 298 K we found, as usual, a linear trend up to 100 bar , so that saturation is not reached. Analogously to methane, when the adsorption per unit mass is considered, higher-density adsorbents are penalized, and in this case the best performance is observed in the lighter structure, independently from the pillar type.

Among the gases considered in this work CH_4 , CO_2 and H_2 are those of major technological interest. We summarize in Tab. 2 and 3 the maximum values of gravimetric and volumetric uptake found for these gases at 1 , 10 and 35 bar , indicating at which pillar type and pillar density corresponds the maximum uptake.

In the case of CH_4 we found a maximum volumetric uptake at 35 bar of $195 \text{ cm}^3(\text{STP})/\text{cm}^3$, with similar performances for different pillar types. This value is comparable with what is observed in MOFs, where methane uptake at the same pressure range is $\approx 230 \text{ cm}^3(\text{STP})/\text{cm}^3$ for the best performer (Mason et al., 2014). The performance of the well-known MOF-5 (IRMOF-1) at the same conditions is $\approx 150 \text{ cm}^3(\text{STP})/\text{cm}^3$.

The amount of CO_2 adsorbed in PGFs is also comparable to what is found in other microporous materials, such as MOFs where gravimetric adsorptions in the range $30\text{--}74.2\%$ are reported at room temperature and pressures up to 50 bar (Sumida et al., 2012). The maximum uptake of CO_2 the PGFs examined is reported in Tab. 3 and can be up to 58.9% at 35 bar in the case of pillar type 3 at the lowest pillar density.

With regards to H_2 we found a maximum value of $\approx 25 \text{ cm}^3(\text{STP})/\text{cm}^3$ for volumetric uptake at 35 bar (Tab. 2) comparable with that of small pore structures such as ZIF-9 and MOF-5 (Garberoglio et al., 2005; Battisti et al., 2011). The value for gravimetric maximum uptake of 0.4% at 35 bar , reported in Tab. 3 is slightly

higher than that of MOF-5 and very similar to that of IRMOF-14 (Garberoglio et al., 2005).

3.2. Comparison between DREIDING and UFF force fields

As already mentioned, the two force fields that are mostly used to estimate dispersion interactions between adsorbed gases and microporous organic materials are DREIDING and UFF, the latter generally resulting in a higher uptake. In order to compare the results obtained by these two force fields in PGFs, we computed

$$R(P) = \frac{N_{\text{ex(UFF)}}(P) - N_{\text{ex(DREIDING)}}(P)}{N_{\text{ex(DREIDING)}}(P)}, \quad (2)$$

where $N_{\text{ex(UFF)}}$ and $N_{\text{ex(DREIDING)}}$ are the excess number of adsorbed molecules at pressure P obtained using UFF force field and DREIDING, respectively. This quantity measures how much adsorption depends on the choice between these two force fields, and is expected to be positive on the basis of the evidence published in literature (Garberoglio et al., 2005; Getman et al., 2012; Sumida et al., 2012).

The values of $R(P)$ in the case of adsorption of CH_4 at 298 K temperature for all the pillar types and three different pillar density are reported in Fig. 8, where one can immediately see that also in the case of PGFs UFF predicts a larger amount of gas adsorbed than DREIDING. The various curves present some clear trends. In particular, $R(P)$ is a decreasing function of the external pressure, reaching values less than 20% at saturation, and an increasing function of pillar density. This is particularly evident at low pressures ($\lesssim 10 \text{ bar}$), where UFF predicts up to twice as much adsorbed amount than DREIDING. In fact, in the low-pressure regime adsorption is mainly determined by the gas-framework interaction, so that the differences between the force fields are emphasized. Conversely, the interaction between gas molecules plays a greater role under saturation conditions (high pressures) and hence the difference due to the two force fields become less important. A similar behavior is observed for CO_2 at 298 K and H_2 at 77 K . Plots corresponding to Fig. 8 can be found in the Supplementary Information.

In the case of H_2 at 298 K instead (Fig. 9), $R(P)$ is essentially constant over the whole pressure range, maintaining the dependence on the pillar type and the pillar density found for the previous cases. This can be explained by the fact that the saturation regime is not reached for H_2 at 298 K , hence the decrease of $R(P)$ at high pressure that is observed in the other gases does not appear in this case.

3.3. Mixture adsorption and selectivity

We investigated the adsorption selectivity of the structures with pillar types 1 and 4 in the case of the following binary mixtures: CH_4/H_2 , CO_2/H_2 , CO_2/CH_4 , N_2/O_2 , CO_2/N_2 . We chose to focus on pillar types 1 and 4 that represent the two extrema as pillar complexity and pillar

	1 bar			10 bar			35 bar		
	uptake (cm ³ (STP)/cm ³)	T	D (nm ⁻²)	uptake (cm ³ (STP)/cm ³)	T	D (nm ⁻²)	uptake (cm ³ (STP)/cm ³)	T	D (nm ⁻²)
CH ₄	43.6	2	1.71	147	4	0.34	195	1	1.02
CO ₂	114	2	1.71	341	4	0.09	360	3	0.09
H ₂	0.81	2	0.09	8.03	2	0.09	24.6	2	0.09

Table 2: Maximum values of volumetric uptake (cm³(STP)/cm³) found for CH₄, CO₂ and H₂ at 1, 10 and 35 bar. For each pressure in the last two columns are indicated the pillar type (T) and pillar density (D) producing the maximum uptake.

	1 bar			10 bar			35 bar		
	uptake (wt%)	T	D (nm ⁻²)	uptake (wt%)	T	D (nm ⁻²)	uptake (wt%)	T	D (nm ⁻²)
CH ₄	3.76	2	1.37	15.2	4	0.09	22.3	3	0.09
CO ₂	22.3	3	1.37	53.5	3	0.09	58.9	3	0.09
H ₂	0.013	3	0.09	0.13	3	0.09	0.40	1	0.09

Table 3: Maximum values of gravimetric uptake found for CH₄, CO₂ and H₂ at 1, 10 and 35 bar. For each pressure in the last two columns are indicated the pillar type (T) and pillar density (D) producing the maximum uptake.

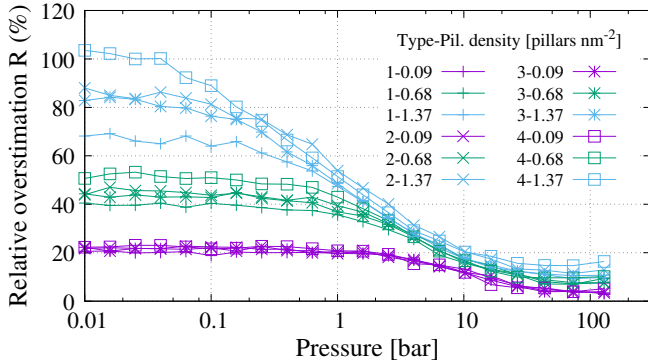


Figure 8: Relative overestimation R of CH₄ adsorption at 298 K using UFF force field in place of DREIDING force field.

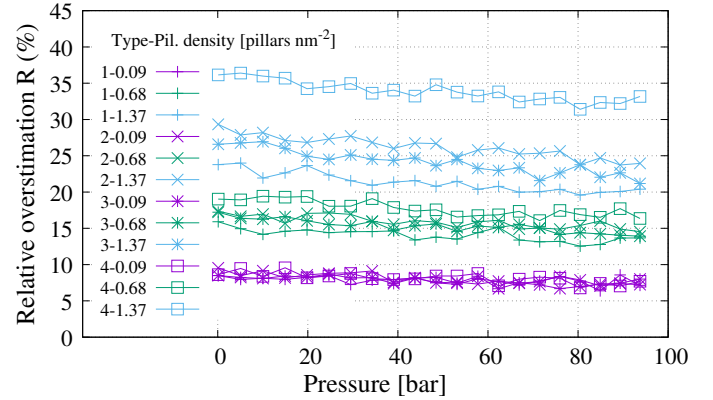


Figure 9: Relative overestimation R of H₂ adsorption at 298 K using UFF force field in place of DREIDING force field.

volume: type-1 pillar is linear and not charged, whereas type-4 pillar has protruding charged moieties (see Fig. 2).

The selectivity of an adsorbent for a mixture of gases is defined by the ratio

$$S(b/a) = \frac{x_b/x_a}{y_b/y_a}, \quad (3)$$

where x_a , x_b denote the molar fractions of the adsorbed species a and b while y_a and y_b denote the molar fractions of the reservoir bulk mixture. In the low-pressure limit the selectivity is independent of the molar composition of the bulk gas. In this case, it can be computed as the ratio of the single-particle partition function of the two species in the adsorbed phase, divided by the ratio of the free-particle partition function of the same two species (Tan and Gubbins, 1992; Challa et al., 2002; Battisti et al., 2011). We denote with S_0 the low-pressure limit of the selectivity.

Values of S_0 are report in Tab. 4 for the pillar densi-

ties of 0.09, 0.68 and 1.37 pillars nm⁻², corresponding to the smallest, the intermediate and the higher values investigated in this work. S_0 is in general dependent on the considered mixture, the pillar density and the pillar type. The zero-pressure selectivity increases with the pillar density for all mixtures, except N₂/O₂ for which it is almost constant. The values of the selectivities for these mixtures are generally comparable to the values reported for other microporous materials, such as MOFs (Garberoglio et al., 2005; Sumida et al., 2012) or ZIFs (Banerjee et al., 2009; Battisti et al., 2011; Prakash et al., 2013).

In general, adsorption selectivities in excess of 100 are considered fairly high. In the case of the structures investigated here, this is observed for the CO₂/H₂ mixture, especially at high pillar densities where we have $S_0(\text{CO}_2/\text{H}_2) \sim 340$. This value is higher than the one found in ZIFs (~ 275 (Battisti et al., 2011)) and also in MOFs, where it reaches the value ~ 100 in CuBTC and

Type	1			4		
Density (nm ⁻²)	0.09	0.68	1.37	0.09	0.68	1.37
CO ₂ /H ₂	26.2	51.4	117.6	35.8	90.2	340.0
CH ₄ /H ₂	9.6	16.2	31.7	12.7	24.6	66.6
CO ₂ /CH ₄	2.7	3.2	3.7	2.8	3.7	5.1
CO ₂ /N ₂	6.3	9.1	14.0	7.1	12.3	27.1
N ₂ /O ₂	1.00	1.02	1.04	1.01	1.02	1.01

Table 4: Zero-pressure adsorption selectivity in the Pillared Graphene Frameworks with pillar types 1 and 4 for different pillar density.

~ 12 in MOF-5 (Yang and Zhong, 2006).

As the selectivity is in general a function of the external pressure, its dependence with respect to this parameter was also considered. We report in Fig. 10 and 11 the pressure dependence of $S(b/a)/S_0$ for the samples with pillar type 1 and 4, respectively, with a density of 0.68 pillars nm⁻². As shown in Fig. 10 and 11 all the mixture selectivities are essentially constant up to 1 bar keeping their low-pressure value. Beyond a few bars we find different trends depending on the mixture: the selectivity can either increase, remain almost constant, or decrease at large pressures with a variation of roughly a factor of two.

The origin of this behavior, which has also been observed in ZIFs (Battisti et al., 2011) can be rationalized using energetic and entropic arguments. For molecules of the same type – e.g. both single Lennard-Jones centers such as CH₄/H₂ or linear rigid rotors such as CO₂/N₂, or N₂/O₂ – the variation in the selectivity is related to the energetic gain upon adsorption at finite pressure. In general, CO₂ is the molecule whose single-particle energy increases the most when the adsorbed density increases. This in turn enhances the probability of another carbon dioxide molecule being adsorbed with respect to its competing species, resulting in an increasing value of the CO₂ selectivity. This is what happens for the CO₂/N₂ and CO₂/CH₄ mixtures: in both cases the energy gain upon adsorption of a carbon dioxide molecule at the highest pressure is ~ 200 K larger than for the adsorption of the other one. This argument applies also in the case of N₂/O₂, where adsorption of an oxygen molecule results in roughly a 25 K gain in energy with respect to the adsorption of a nitrogen one. As a consequence, the selectivity decreases at higher pressures.

However, this picture seem to be in contrast with what is observed in the case of the CO₂/H₂ mixture, whose selectivity shows only a modest increase at the highest pressure despite the fact that CO₂ adsorption is favored by ~ 100 K gain in energy. In this case one should also take into account the fact that upon adsorption, especially in packed geometries, a carbon dioxide molecule can become rotationally hindered. This loss of entropy balances the gain of energy, resulting in a modest 20% gain in selectivity at

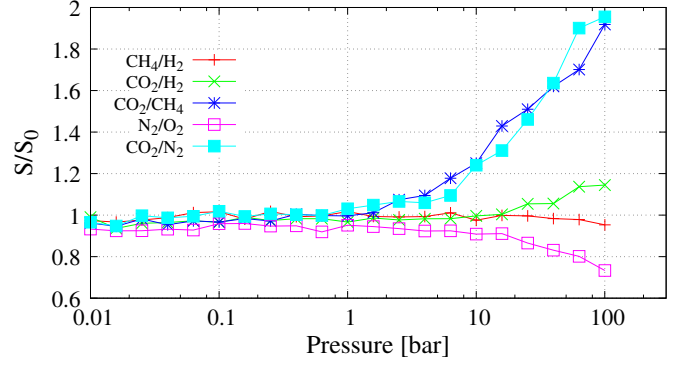


Figure 10: Selectivity for gas mixtures at T= 298 K, normalized with respect to the zero-pressure limit value of selectivity (S_0), for the sample with pillar type 1 and pillar density 0.68 pillars nm⁻².

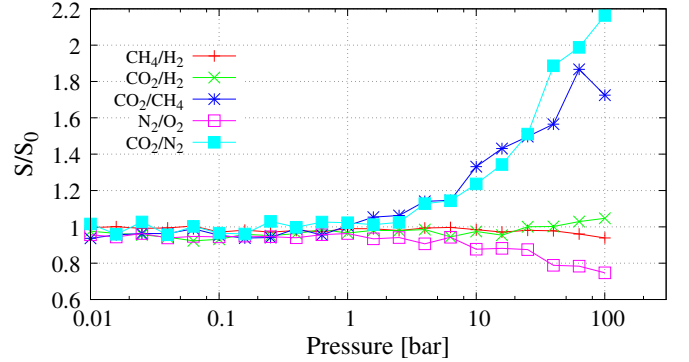


Figure 11: Selectivity for gas mixtures at T= 298 K, normalized with respect to the zero-pressure limit value of selectivity (S_0), for the sample with pillar type 4 and pillar density 0.68 pillars nm⁻².

high pressures. To check this we performed calculations at the lowest and highest pillar densities: in the former case the CO₂/H₂ selectivity increases by up to 50%, in the latter it remains constant (within the uncertainties of the calculation).

3.4. Dynamics of adsorbed molecules and permeation selectivity

The simulation of gas dynamics was performed using MD simulations within LAMMPS code (Plimpton, 1995). The framework topologies to be used in LAMMPS code were generated according to the bonded part of UFF using a modified version of OBGIMX (Garberoglio, 2012). We started from representative configuration of pure gas adsorption at two different pressures for which the adsorption uptake was maximum and half maximum. For H₂ at 298 K we take as maximum the 100 bar point.

The isothermal simulations started with a 500 ps equilibration at T = 298 K driven by a Nosé-Hoover thermostat with a time constant $\tau = 1$ ps. The x , y and z components of the mean-squared displacement were com-

puted and averaged over 10 consecutive 500 ps MD trajectories, in which the thermostat coupling time was reduced to $\tau = 50$ ps.

The diffusion coefficients were calculated by means of a weighted least square fit of 100 ps separated points of the averaged mean-squared displacement curve. Indeed the diffusion coefficient can be computed from the mean-squared displacement curve as

$$D_x = \lim_{t \rightarrow +\infty} \frac{1}{2} \frac{d\Delta x^2(t)}{dt}, \quad (4)$$

with an analogous definition for the y and z directions. Due to the fact that all the samples present no gas diffusion in the direction perpendicular to the graphene planes, the overall diffusion coefficient can be assessed as the average between the x and the y directions,

$$D = \frac{1}{2}(D_x + D_y). \quad (5)$$

As a first test, we checked the effect of framework flexibility on the values of the self-diffusion coefficient in Eq. (5), considering the case of CH_4 and CO_2 moving in PGFs with pillar density 0.09 and 1.37 pillars nm^{-2} , pillar type 1 and 4, at maximum and half maximum gravimetric uptake. We found a relative difference in D between mobile and fixed framework of 5 – 15 % and 30 – 40 % for pillar density 0.09 and 1.374 pillars nm^{-2} , respectively. Given these results, we decided to use a flexible model of the framework in the calculation of self-diffusion.

Type		1			4		
Density (nm^{-2})		0.09	0.68	1.37	0.09	0.68	1.37
CH_4	H	30.3	12.9	3.32	35.9	7.84	0.617
	M	14.3	6.96	2.34	10.6	4.09	0.538
CO_2	H	4.04	2.85	1.27	9.56	1.60	0.270
	M	0.941	0.696	0.360	0.825	1.34	0.113
H_2	H	219	74.3	23.6	170	38.4	4.07
	M	129	49.5	20.0	105	27.8	2.79
N_2	H	23.3	10.6	4.55	15.4	5.26	0.870
	M	6.30	3.69	1.89	4.53	2.22	0.531
O_2	H	28.5	11.7	5.48	23.1	5.88	1.13
	M	8.49	4.27	2.67	5.97	2.81	0.58

Table 5: Diffusion coefficients (in units of $10^{-8} \text{ m}^2 \text{ s}^{-1}$) for the Pillared Graphene Frameworks with pillar types 1 and 4 for different pillar density at half maximum (H) and maximum (M) gravimetric uptake.

The results for diffusion coefficient for pillar types number 1 and 4 with pillar density 0.09, 0.68 and 1.37 pillars nm^{-2} are reported in Tab. 5. The general trend is a decrease of the self-diffusion coefficient with increasing pillar density.

Furthermore, H_2 is the gas with higher diffusion values followed by CH_4 , N_2 and O_2 with similar values, and

finally CO_2 with the lower diffusion coefficients. This sorting is largely independent of the pillar type or density.

The diffusion coefficients reported in Tab. 5 are all higher than $10^{-9} \text{ m}^2 \text{ s}^{-1}$, the order of magnitude of self-diffusion coefficient in liquid such as H_2O , so that none of the considered structures inhibits gas diffusion. However, for pillar density higher than 1.37 pillars nm^{-2} , the gas diffusion could be hindered. Differently from ZIFs and MOFs, in which the structures with small windows connecting the pores, such as, for example, ZIF-5 and ZIF-9 (Battisti et al., 2011), can easily inhibit the gas diffusion, in PGFs the diffusion is not hindered even at high pillar density because the pore are constituted by the free volume between mobile moieties and there are no definite windows to be crossed.

Type	1			4		
Density (nm ⁻²)	0.09	0.68	1.37	0.09	0.68	1.37
CO ₂ /H ₂	0.48	1.97	6.30	2.01	3.76	22.6
CH ₄ /H ₂	1.33	2.83	4.46	2.68	5.02	10.1
CO ₂ /CH ₄	0.36	0.70	1.41	0.75	0.75	2.23
CO ₂ /N ₂	1.09	2.44	3.89	4.38	3.75	8.39
N ₂ /O ₂	0.81	0.92	0.87	0.67	0.91	0.78

Table 6: Separation performance factor $\Sigma = \Sigma_0 \Pi$ for the Pillared Graphene Frameworks with pillar types 1 and 4 for different pillar density.

The overall performance of PGFs for gas separation is determined by a tradeoff between high adsorption selectivity (which is enhanced by high pillar densities, see Tab. 4) and molecular transport (which is hindered by high pillar densities, see Tab. 5). A quantity taking into account this two opposite density regimes is the so called permeance selectivity Σ which is defined as the product

$$\Sigma = \Sigma_0 \Pi, \quad (6)$$

where Σ_0 is the low-pressure selectivity and Π is the ratio between the self-diffusion coefficients of the two gases (Krishna and van Baten, 2007; Liu and Johnson, 2009; Battisti et al., 2011).

The results for separation performance factor for pillar types number 1 and 4 with pillar density 0.09, 0.68 and 1.37 pillars nm^{-2} are reported in Tab. 6. To compute the separation performance factor the diffusion coefficients at half maximum of gravimetric uptake were used.

As general trend the separation performance factor for a given mixture increases as the pillar density increases. We found good performances for the high pillar density samples for CO_2/H_2 and CH_4/H_2 with maximum values of 22.6 and 10.1, respectively. These values are significantly larger than the ones found in the analysis of gas separation in ZIFs (Battisti et al., 2011) where values of 3.42 and 1.42 were observed. Inspection of the values of S_0 and Π show that the origin of the higher performance of PGFs is mainly due to their larger value of S_0 , since the ratio of

the diffusion coefficient leading to Π is roughly the same for PGFs and ZIFs.

A value of $\Sigma = 8.39$ was also found for CO_2/N_2 separation. For this mixture, ZIFs were found to have a maximum value $\Sigma = 10.4$, in the case of ZIF-4 (Battisti et al., 2011). For this particular mixture, PGFs have a slightly less performing separation behavior, despite having a larger value of S_0 (27.1 versus 8.2) due to the fact that the self-diffusion coefficient of N_2 is three times higher than that of CO_2 in PGFs. In the case of ZIF-4, the value of Π turns out to be ~ 1 (Battisti et al., 2011).

4. Conclusions

In this paper we presented an extensive analysis of gas adsorption and separation for nitrogen-containing Pillared Graphene Frameworks using computer simulations. In particular, we focused on the influence of the pillar type and the pillar density on the performance for gas storage and separation. We took into account the quadrupole moment of CO_2 , H_2 and O_2 molecules. Furthermore, we used the self consistent point charges extracted by ReaxFF simulations to model the Coulomb interactions between the gases and the frameworks.

Our results show that the density of pillars has a greater influence on adsorption than the pillar type. Under saturation conditions, the increase of pillar density results in a sensible decrease of the amount of gas adsorbed. Despite this shortcoming, the absolute value of the amount adsorbed is comparable to what is observed in organic frameworks (MOFs, ZIFs or COFs), although it falls short to achieving the performance of the best of them.

In the case of adsorption selectivity, we found that one can have a lot of control on the performance by varying both the pillar type and density. The actual range of variability, though, depends on the specific mixture under consideration. In the case of CO_2/H_2 , the ratio between the maximum and minimum adsorption selectivity at zero-pressure (see Tab. 4) is more than factor of ten. Conversely, the selectivity of the N_2/O_2 mixture is always close to one, irrespectively on the nature of the pillar considered or its density. However, selectivity is in general an increasing function of the pillar density.

When dynamical properties are considered, the effect of pillar density is very pronounced. In general we found roughly an inverse proportionality between the pillar density and the self-diffusion coefficient. This finding paves the way to the possibility of tailoring transport properties to a high degree of precision, possibly up to the ballistic regime. However, there might be issues of stability of the Pillared Graphene Structure at very low pillar densities that will have to be addressed.

Finally, when the overall separation performance Σ – which includes both adsorption and diffusion – is considered, PGFs show quite a good performance when compared with other microporous materials, especially in the case of the CO_2/H_2 and CH_4/H_2 mixtures.

Acknowledgements

We thank prof. Marco Frascioni for advice on the kind of moieties to be used as pillars. N.M.P. is supported by the European Research Council PoC 2015 “Silkene” No. 693670, by the European Commission H2020 under the Graphene Flagship Core 1 No. 696656 (WP14 “Polymer Nanocomposites”) and under the Fet Proactive “Neurofibres” No.732344. S.T and G.G. acknowledge funding from previous WP14 “Polymer Nanocomposites” grant. Access to computing and storage facilities owned by parties and projects contributing to the Czech National Grid Infrastructure MetaCentrum provided under the programme “Projects of Large Research, Development, and Innovations Infrastructures” (CESNET LM2015042), is greatly appreciated (<https://www.metacentrum.cz/en/>).

References

- Alonso, J.A.C., 2012. The Storage of Hydrogen in Nanoporous Carbons. *Journal of the Mexican Chemical Society* 56, 261 – 269. URL: http://www.scielo.org.mx/scielo.php?script=sci_arttext&pid=S1870-249X2012000300006&nrm=iso.
- Amirjalayer, S., Tafipolsky, M., Schmid, R., 2007. Molecular dynamics simulation of benzene diffusion in mof-5: Importance of lattice dynamics. *Angewandte Chemie International Edition* 46, 463–466. URL: <http://dx.doi.org/10.1002/anie.200601746>, doi:10.1002/anie.200601746.
- Babarao, R., Hu, Z., Jiang, J., Chempath, S., Sandler, S.I., 2007. Storage and separation of CO_2 and CH_4 in silicalite, c168 schwarzite, and 1rmof-1a: a comparative study from monte carlo simulation. *Langmuir* 23, 659–666. URL: <http://dx.doi.org/10.1021/la062289p>, doi:10.1021/la062289p, arXiv:<http://dx.doi.org/10.1021/la062289p>.
- Banerjee, R., Furukawa, H., Britt, D., Knobler, C., O’Keeffe, M., Yaghi, O.M., 2009. Control of pore size and functionality in isoreticular zeolitic imidazolate frameworks and their carbon dioxide selective capture properties. *Journal of the American Chemical Society* 131, 3875–3877. URL: <http://dx.doi.org/10.1021/ja809459e>, doi:10.1021/ja809459e, arXiv:<http://dx.doi.org/10.1021/ja809459e>. PMID: 19292488.
- Battisti, A., Taioli, S., Garberoglio, G., 2011. Zeolitic imidazolate frameworks for separation of binary mixtures of CO_2 , CH_4 , N_2 and H_2 : A computer simulation investigation. *Microporous and Mesoporous Materials* 143, 46 – 53. URL: <http://www.sciencedirect.com/science/article/pii/S138718111100045X>, doi:<http://dx.doi.org/10.1016/j.micromeso.2011.01.029>.
- Buch, V., 1994. Path integral simulations of mixed para-d2 and ortho-d2 clusters: The orientational effects. *The Journal of Chemical Physics* 100, 7610–7629. URL: <http://dx.doi.org/10.1063/1.466854>, doi:10.1063/1.466854, arXiv:<http://dx.doi.org/10.1063/1.466854>.
- Burress, J.W., Gadipelli, S., Ford, J., Simmons, J.M., Zhou, W., Yildirim, T., 2010. Graphene oxide framework materials: Theoretical predictions and experimental results. *Angewandte Chemie International Edition* 49, 8902–8904. URL: <http://dx.doi.org/10.1002/anie.201003328>, doi:10.1002/anie.201003328.
- Challa, S.R., Sholl, D.S., Johnson, J.K., 2002. Adsorption and separation of hydrogen isotopes in carbon nanotubes: Multicomponent grand canonical monte carlo simulations. *The Journal of Chemical Physics* 116, 814–824. URL: <http://dx.doi.org/10.1063/1.1423665>, doi:10.1063/1.1423665, arXiv:<http://dx.doi.org/10.1063/1.1423665>.
- Chenoweth, K., van Duin, A.C.T., Goddard, W.A., 2008. Reaxff reactive force field for molecular dynamics simulations of hydrocarbon oxidation. *The Journal of Physical Chemistry A* 112, 1040–

1053. URL: <http://dx.doi.org/10.1021/jp709896w>, doi:10.1021/jp709896w, arXiv:<http://dx.doi.org/10.1021/jp709896w>.
- Colon, Y.J., Snurr, R.Q., 2014. High-throughput computational screening of metal-organic frameworks. *Chem. Soc. Rev.* 43, 5735–5749. URL: <http://dx.doi.org/10.1039/C4CS00070F>, doi:10.1039/C4CS00070F.
- Coluci, V.R., Braga, S.F., Baughman, R.H., Galvão, D.S., 2007. Prediction of the hydrogen storage capacity of carbon nanoscrolls. *Phys. Rev. B* 75, 125404. URL: <https://link.aps.org/doi/10.1103/PhysRevB.75.125404>, doi:10.1103/PhysRevB.75.125404.
- Ding, F., Lin, Y., Krasnov, P.O., Yakobson, B.I., 2007. Nanotube-derived carbon foam for hydrogen sorption. *J. Chem. Phys.* 127, 164703. URL: <http://dx.doi.org/10.1063/1.2790434>, doi:10.1063/1.2790434.
- van Duin, A.C.T., Dasgupta, S., Lorant, F., Goddard, W.A., 2001. Reaxff: a reactive force field for hydrocarbons. *The Journal of Physical Chemistry A* 105, 9396–9409. URL: <http://dx.doi.org/10.1021/jp004368u>, doi:10.1021/jp004368u, arXiv:<http://dx.doi.org/10.1021/jp004368u>.
- Duren, T., Bae, Y.S., Snurr, R.Q., 2009. Using molecular simulation to characterise metal-organic frameworks for adsorption applications. *Chem. Soc. Rev.* 38, 1237–1247. URL: <http://dx.doi.org/10.1039/B803498M>, doi:10.1039/B803498M.
- Duren, T., Sarkisov, L., Yaghi, O.M., Snurr, R.Q., 2004. Design of new materials for methane storage. *Langmuir* 20, 2683–2689. URL: <http://dx.doi.org/10.1021/la0355500>, doi:10.1021/la0355500, arXiv:<http://dx.doi.org/10.1021/la0355500>.
- Garberoglio, G., 2012. Obgmx: A web-based generator of gromacs topologies for molecular and periodic systems using the universal force field. *Journal of Computational Chemistry* 33, 2204–2208. URL: <http://dx.doi.org/10.1002/jcc.23049>, doi:10.1002/jcc.23049.
- Garberoglio, G., Pugno, N.M., Taioli, S., 2015. Gas adsorption and separation in realistic and idealized frameworks of organic pillared graphene: A comparative study. *The Journal of Physical Chemistry C* 119, 1980–1987. URL: <http://dx.doi.org/10.1021/jp511953p>, doi:10.1021/jp511953p.
- Garberoglio, G., Skoulidas, A.I., Johnson, J.K., 2005. Adsorption of gases in metal organic materials: comparison of simulations and experiments. *The Journal of Physical Chemistry B* 109, 13094–13103. URL: <http://dx.doi.org/10.1021/jp0509481>, doi:10.1021/jp0509481, arXiv:<http://dx.doi.org/10.1021/jp0509481>.
- Garberoglio, G., Taioli, S., 2012. Modeling flexibility in metal-organic frameworks: Comparison between density-functional tight-binding and universal force field approaches for bonded interactions. *Microporous and Mesoporous Materials* 163, 215 – 220. URL: <http://www.sciencedirect.com/science/article/pii/S1387181112004581>, doi:<https://doi.org/10.1016/j.micromeso.2012.07.026>.
- Getman, R.B., Bae, Y.S., Wilmer, C.E., Snurr, R.Q., 2012. Review and analysis of molecular simulations of methane, hydrogen, and acetylene storage in metal-organic frameworks. *Chemical Reviews* 112, 703–723. URL: <http://dx.doi.org/10.1021/cr200217c>, doi:10.1021/cr200217c, arXiv:<http://dx.doi.org/10.1021/cr200217c>.
- Goodbody, S.J., Watanabe, K., MacGowan, D., Walton, J.P.R.B., Quirke, N., 1991. Molecular simulation of methane and butane in silicalite. *J. Chem. Soc., Faraday Trans.* 87, 1951–1958. URL: <http://dx.doi.org/10.1039/FT9918701951>, doi:10.1039/FT9918701951.
- Haldoupis, E., Nair, S., Sholl, D.S., 2010. Efficient calculation of diffusion limitations in metal organic framework materials: A tool for identifying materials for kinetic separations. *Journal of the American Chemical Society* 132, 7528–7539. URL: <http://dx.doi.org/10.1021/ja1023699>, doi:10.1021/ja1023699, arXiv:<http://dx.doi.org/10.1021/ja1023699>, PMID: 20450176.
- Harris, J.G., Yung, K.H., 1995. Carbon dioxide's liquid-vapor coexistence curve and critical properties as predicted by a simple molecular model. *The Journal of Physical Chemistry* 99, 12021–12024. URL: <http://dx.doi.org/10.1021/j100031a034>, doi:10.1021/j100031a034, arXiv:<http://dx.doi.org/10.1021/j100031a034>.
- Hertag, L., Bux, H., Caro, J., Chmelik, C., Remsungnen, T., Knauth, M., Fritzsche, S., 2011. Diffusion of ch₄ and h₂ in zif-8. *Journal of Membrane Science* 377, 36 – 41. URL: <http://www.sciencedirect.com/science/article/pii/S037673881100024X>, doi:<https://doi.org/10.1016/j.memsci.2011.01.019>.
- Hirschfelder, J., Curtiss, C., 1954. Rb bird molecular theory of liquids and gases.
- Krishna, R., van Baten, J., 2007. Using molecular simulations for screening of zeolites for separation of co₂/ch₄ mixtures. *Chemical Engineering Journal* 133, 121 – 131. URL: <http://www.sciencedirect.com/science/article/pii/S1385894707001106>, doi:<http://dx.doi.org/10.1016/j.cej.2007.02.011>.
- Kumar, R., Suresh, V.M., Maji, T.K., Rao, C.N.R., 2014. Porous graphene frameworks pillared by organic linkers with tunable surface area and gas storage properties. *Chem. Commun.* 50, 2015–2017. URL: <http://dx.doi.org/10.1039/C3CC46907G>, doi:10.1039/C3CC46907G.
- Liu, J., Johnson, J.K., 2009. Prediction of ch₄/h₂ mixture selectivity in zn(tbp) from computer simulations. *Journal of Low Temperature Physics* 157, 268–276. URL: <http://dx.doi.org/10.1007/s10909-009-9910-2>, doi:10.1007/s10909-009-9910-2.
- Mason, J.A., Veenstra, M., Long, J.R., 2014. Evaluating metal-organic frameworks for natural gas storage. *Chem. Sci.* 5, 32–51. URL: <http://dx.doi.org/10.1039/C3SC52633J>, doi:10.1039/C3SC52633J.
- Mattsson, T.R., Lane, J.M.D., Cochrane, K.R., Desjarlais, M.P., Thompson, A.P., Pierce, F., Grest, G.S., 2010. First-principles and classical molecular dynamics simulation of shocked polymers. *Phys. Rev. B* 81, 054103. URL: <https://link.aps.org/doi/10.1103/PhysRevB.81.054103>, doi:10.1103/PhysRevB.81.054103.
- Mayo, S.L., Olafson, B.D., Goddard, W.A., 1990. Dreiding: a generic force field for molecular simulations. *The Journal of Physical Chemistry* 94, 8897–8909. URL: <http://dx.doi.org/10.1021/j100389a010>, doi:10.1021/j100389a010, arXiv:<http://dx.doi.org/10.1021/j100389a010>.
- Mpourmpakis, G., Tzilianakis, E., Froudakis, G.E., 2007. Carbon nanoscrolls: a promising material for hydrogen storage. *Nano Letters* 7, 1893–1897. URL: <http://dx.doi.org/10.1021/nl070530u>, doi:10.1021/nl070530u, arXiv:<http://dx.doi.org/10.1021/nl070530u>.
- Murthy, C., Singer, K., Klein, M., McDonald, I., 1980. Pairwise additive effective potentials for nitrogen. *Molecular Physics* 41, 1387–1399. URL: <http://dx.doi.org/10.1080/00268978000103611>, doi:10.1080/00268978000103611, arXiv:<http://dx.doi.org/10.1080/00268978000103611>.
- Nakano, A., 1997. Parallel multilevel preconditioned conjugate-gradient approach to variable-charge molecular dynamics. *Computer Physics Communications* 104, 59 – 69. URL: <http://www.sciencedirect.com/science/article/pii/S0010465597000416>, doi:[http://dx.doi.org/10.1016/S0010-4655\(97\)00041-6](http://dx.doi.org/10.1016/S0010-4655(97)00041-6).
- Pantatosaki, E., Megariotis, G., Pusch, A.K., Chmelik, C., Stallmach, F., Papadopoulos, G.K., 2012. On the impact of sorbent mobility on the sorbed phase equilibria and dynamics: A study of methane and carbon dioxide within the zeolite imidazolate framework-8. *The Journal of Physical Chemistry C* 116, 201–207. URL: <http://dx.doi.org/10.1021/jp207771s>, doi:10.1021/jp207771s, arXiv:<http://dx.doi.org/10.1021/jp207771s>.
- Pedrielli, A., Taioli, S., Garberoglio, G., Pugno, N.M., 2017. Designing graphene based nanofoams with nonlinear auxetic and anisotropic mechanical properties under tension or compression. *Carbon* 111, 796 – 806. URL: <http://www.sciencedirect.com/science/article/pii/S0008622316308946>, doi:<https://doi.org/10.1016/j.carbon.2016.10.034>.
- Plimpton, S., 1995. Fast parallel algorithms for short-range molecular dynamics. *Journal of Computational Physics* 117, 1–19. URL: <http://dx.doi.org/10.1006/jcph.1995.1039>, doi:10.1006/jcph.1995.1039.
- Prakash, M., Sakhavand, N., Shahsavari, R., 2013. H₂, n₂, and ch₄ gas adsorption in zeolitic imidazolate framework-95 and -100: Ab initio based grand canonical monte carlo simulations. *The Journal of Physical Chemistry C* 117, 24407–24416. URL:

- <http://dx.doi.org/10.1021/jp408075y>, doi:10.1021/jp408075y, arXiv:<http://dx.doi.org/10.1021/jp408075y>.
- Rappé, A.K., Casewit, C.J., Colwell, K.S., Goddard, W.A., Skiff, W.M., 1992. Uff, a full periodic table force field for molecular mechanics and molecular dynamics simulations. *Journal of the American Chemical Society* 114, 10024–10035. URL: <http://dx.doi.org/10.1021/ja00051a040>, doi:10.1021/ja00051a040, arXiv:<http://dx.doi.org/10.1021/ja00051a040>.
- Rappé, A.K., Goddard, W.A., 1991. Charge equilibration for molecular dynamics simulations. *The Journal of Physical Chemistry* 95, 3358–3363. URL: <http://dx.doi.org/10.1021/j100161a070>, doi:10.1021/j100161a070, arXiv:<http://dx.doi.org/10.1021/j100161a070>.
- Srinivas, G., Burrell, J.W., Ford, J., Yildirim, T., 2011. Porous graphene oxide frameworks: Synthesis and gas sorption properties. *J. Mater. Chem.* 21, 11323–11329. URL: <http://dx.doi.org/10.1039/C1JM11699A>, doi:10.1039/C1JM11699A.
- Sumida, K., Rogow, D.L., Mason, J.A., McDonald, T.M., Bloch, E.D., Herm, Z.R., Bae, T.H., Long, J.R., 2012. Carbon dioxide capture in metal–organic frameworks. *Chemical Reviews* 112, 724–781. URL: <http://dx.doi.org/10.1021/cr2003272>, doi:10.1021/cr2003272, arXiv:<http://dx.doi.org/10.1021/cr2003272>.
- Tan, Z., Gubbins, K.E., 1992. Selective adsorption of simple mixtures in slit pores: a model of methane-ethane mixtures in carbon. *The Journal of Physical Chemistry* 96, 845–854. URL: <http://dx.doi.org/10.1021/j100181a059>, doi:10.1021/j100181a059, arXiv:<http://dx.doi.org/10.1021/j100181a059>.
- Tang, Q., Zhou, Z., Chen, Z., 2013. Graphene-related nanomaterials: tuning properties by functionalization. *Nanoscale* 5, 4541–4583. URL: <http://dx.doi.org/10.1039/C3NR33218G>, doi:10.1039/C3NR33218G.
- Wang, X., Sun, G., Chen, P., 2014. Three-dimensional porous architectures of carbon nanotubes and graphene sheets for energy applications. *Frontiers in Energy Research* 2. URL: http://www.frontiersin.org/nanoenergy_technologies_and_materials/10.3389/fenrg.2014.00033/abstract, doi:10.3389/fenrg.2014.00033.
- Yang, Q., Zhong, C., 2006. Molecular simulation of carbon dioxide/methane/hydrogen mixture adsorption in metal–organic frameworks. *The Journal of Physical Chemistry B* 110, 17776–17783. URL: <http://dx.doi.org/10.1021/jp062723w>, doi:10.1021/jp062723w, arXiv:<http://dx.doi.org/10.1021/jp062723w>. PMID: 16956262.
- Zhang, L., Hu, Z., Jiang, J., 2013. Sorption-induced structural transition of zeolitic imidazolate framework-8: A hybrid molecular simulation study. *Journal of the American Chemical Society* 135, 3722–3728. URL: <http://dx.doi.org/10.1021/ja401129h>, doi:10.1021/ja401129h, arXiv:<http://dx.doi.org/10.1021/ja401129h>.
- Zhang, L., Siepmann, J.I., 2006. Direct calculation of henry’s law constants from gibbs ensemble monte carlo simulations: nitrogen, oxygen, carbon dioxide and methane in ethanol. *Theoretical Chemistry Accounts* 115, 391–397. URL: <http://dx.doi.org/10.1007/s00214-005-0073-1>, doi:10.1007/s00214-005-0073-1.
- Zhang, L., Wu, G., Jiang, J., 2014. Adsorption and diffusion of co₂ and ch₄ in zeolitic imidazolate framework-8: Effect of structural flexibility. *The Journal of Physical Chemistry C* 118, 8788–8794. URL: <http://dx.doi.org/10.1021/jp500796e>, doi:10.1021/jp500796e, arXiv:<http://dx.doi.org/10.1021/jp500796e>.